FUSION OF POLARIMETRIC RADAR IMAGES USING HYBRID MATCHING PURSUIT

Cong Peng [1], Gang Li [2] and Robert J. Burkholder [3]

1. Shenzhen Institute of Information Technology, Shenzhen, Guangdong 518172, China
2. Tsinghua University, Beijing 100084, China
3. The Ohio State University, Columbus, OH 43212, USA

ABSTRACT

In this paper, we consider the problem of fusion of multi-polarization radar images and develop a new greedy algorithm referred to as hybrid matching pursuit (HMP). By combining the strengths of the orthogonal matching pursuit algorithm and the subspace pursuit algorithm, HMP can enhance target reflections and attenuate background clutter. Experimental results based on measured radar data demonstrate that HMP offers better image quality with higher target-clutter-ratio compared to some popular greedy algorithms.

Index Terms—polarimetric radar, compressive sensing, joint sparsity pattern, microwave imaging, image fusion

1. INTRODUCTION

Polarization diversity has been successfully utilized to improve the performance of radar target detection and classification [1]-[9]. Since a target has different scattering behavior for different polarizations, multi-polarization sensing contains more valuable information that single polarization does not provide. A typical example is the fusion of multi-polarization radar images [10]-[12], in which the source images acquired from different polarimetric channels are combined into one single image to obtain a clearer and less cluttered interpretation of the observed scene.

The traditional methods for radar image formation such as back-projection (BP) or delay-and-sum beamforming are based on matched filtering of all the spatial and temporal measurements, in which high down-range resolution is obtained by employing ultra-wideband waveforms and high cross-range resolution comes from a large antenna aperture. Regarding the fusion of source images, commonly used techniques include pixel-wise arithmetic fusion such as additive [13] and multiplicative [14] operations, principal component analysis (PCA) fusion [15], wavelet transform fusion [16], and fuzzy fusion [11][12]. The fusion methods based on multiplication, PCA and the wavelet transform may suffer from performance loss in multi-polarization radar image fusion scenarios, since the source images from different polarimetric channels may provide inconsistent scattering representations of the observed targets. The above traditional methods require a large number of measurements to preserve the qualities of the source images from all the polarimetric channels.

Recently, the compressive sensing (CS) technique has been applied to radar image formation. From the viewpoint of CS, the task of radar image fusion can be naturally formulated as the problem of jointly sparse signal recovery under the multiple measurement vectors (MMV) model. MMV enforces a common sparsity pattern for all the source images and, therefore, promotes the consistency of content in the source images. The combination of MMV with the fusion of radar images has been investigated in [17]-[20], where linear programing and Bayesian learning are used to form the sparse images from each channel.

In this paper, we consider the problem of fusion of multi-polarization radar images via greedy algorithms. Generally speaking, greedy algorithms are more computationally efficient than methods based on linear programing and Bayesian learning. We develop a new greedy algorithm, hybrid matching pursuit (HMP), by combining the strengths of the orthogonal matching pursuit (OMP) algorithm [23] and the subspace pursuit (SP) algorithm [22] for fusion of multi-polarization radar images. The source images are generated by independently performing OMP on the local data from each polarimetric channel. By following the backtracking strategy of SP, the fusion of all the local sparse solutions is carried out to obtain the global estimate of the common support set. Experimental results show that, compared to some popular greedy algorithms including simultaneous OMP (SOMP) [21], joint OMP (JOMP) [24] and simultaneous subspace pursuit (SSP) [25], HMP offers better quality of fusion of multi-polarization radar images with higher target-to-clutter ratio (TCR).

This work was supported in part by the National Natural Science Foundation of China under Grants 61422110 and 41271011, and in part by the Program for New Century Excellent Talents in University under Grant NCET-11-0270, and in part by the Tsinghua University Initiative Scientific Research Program.

2. SIGNAL MODEL

Assume that the observed scene occupies a volume V. The location of a voxel is denoted by the displacement vector from the origin to the voxel $\overline{r}$. Suppose that the radar data are collected by an antenna at M positions $\{\overline{r}_1,\cdots\overline{r}_m,\cdots,\overline{r}_M\}$ and at L frequency points $\{f_1,\cdots,f_l,\cdots,f_L\}$. Using the Born model, the signal of the q-th polarimetric channel received at the m-th position and at the l-th frequency point can be expressed as

$$s_m^{(q)}(l)=\int_V \sigma^{(q)}(\overline{r})e^{-j4\pi f_l|\overline{r}-\overline{r}_m|/c}dV\ , \quad (1)$$

where $\sigma^{(q)}(\overline{r})$ is the radar reflectivity of the voxel $\overline{r}$ from the q-th polarimetric channel, and c is the propagation speed. The down-range amplitude spread of each scatterer and the antenna pattern have been included in $\sigma^{(q)}(\overline{r})$. The frequency response characteristic of each scatterer in the scene is assumed to be constant over the frequency band. For full-polarization radar, the measurement data at four polarizations are available, i.e., the values of q from 1 to 4 correspond to HH, VV, HV and VH polarizations, respectively. It is worth mentioning that the value of $\sigma^{(q)}(\overline{r})$ may vary with different values of q, i.e., a target may show quite different scattering characteristics at different polarizations.

We discretize the observed volume V as $N_x\times N_y\times N_z$ voxels and assume that $M^{(q)}$ positions and $L^{(q)}$ frequency points are available at the q-th polarimetric channel. Then, (1) can be rewritten as the MMV model:

$$\mathbf{s}^{(q)}=\mathbf{\Phi}^{(q)}\boldsymbol{\sigma}^{(q)}+\mathbf{w}^{(q)}, \quad (2)$$

where $\mathbf{s}^{(q)}=[s_1^{(q)}(1),\cdots,s_{M^{(q)}}^{(q)}(L^{(q)})]^T\in\mathbb{C}^{M^{(q)}L^{(q)}\times 1}$ includes the measurements of the q-th polarimetric channel collected at $M^{(q)}$ positions and $L^{(q)}$ frequency points, $(\cdot)^T$ denotes transpose operation, $\boldsymbol{\sigma}^{(q)}\in\mathbb{C}^{N_xN_yN_z\times 1}$ is the discrete version of the reflectivity density function of the observed volume at the q-th polarimetric channel, and $\mathbf{w}^{(q)}\in\mathbb{C}^{M^{(q)}L^{(q)}\times 1}$ is additive noise and the scattering contributions from outside V at the q-th polarimetric channel. The dictionary matrix is $\mathbf{\Phi}^{(q)}\in\mathbb{C}^{M^{(q)}L^{(q)}\times N_xN_yN_z}$ and its elements are given by,

$$\begin{aligned}&\mathbf{\Phi}^{(q)}\left(l+(m-1)L,n_x+(n_y-1)N_x+(n_z-1)N_xN_y\right)\\&=e^{-j4\pi f_l\left|\overline{r}_{n_x,n_y,n_z}-\overline{r}_m\right|/c}\end{aligned}, \quad (3)$$

where $\overline{r}_{n_x,n_y,n_z}$ represents the position of the voxel with coordinates (n_x,n_y,n_z), $n_x=1,2,\cdots,N_x$, $n_y=1,2,\cdots,N_y$, and $n_z=1,2,\cdots,N_z$. Since we take the same rule of discretization of the observed volume at different polarimetric channels, $\{\boldsymbol{\sigma}^{(q)},q=1,2,3,4\}$ have the same sparsity pattern. The set consisting of the indices corresponding to non-zero coefficients is defined as the common support set, i.e, $\Lambda=\{i:\boldsymbol{\sigma}^{(q)}(i)\neq 0,i=1,2,\cdots,N_xN_yN_z\}$. Denote K as the common sparsity, i.e., $|\Lambda|=K$. Without loss of generality, we assume $2K\le M^{(q)}L^{(q)}<N_xN_yN_z$, for q=1,2,3,4. The fusion of multi-polarization radar images can be carried out by first estimating Λ and then taking average over $\{\boldsymbol{\sigma}^{(q)}(\Lambda),q=1,2,3,4\}$.

3. ALGORITHM DESCRIPTION

The HMP algorithm is summarized in Algorithm 1. Similar to existing greedy algorithms, the HMP algorithm also aims to recover the common support set in an iterative fashion. In the initialization phase, the sparse solution is obtained by independently applying the standard OMP algorithm at each polarimetric channel. This progress is denoted by $\hat{\boldsymbol{\sigma}}_{omp}^{(q)}=\mathrm{OMP}(\mathbf{s}^{(q)},\mathbf{\Phi}^{(q)},K)$, where $\hat{\boldsymbol{\sigma}}_{omp}^{(q)}\in\mathbb{C}^{N_xN_yN_z\times 1}$ and its K nonzero entries correspond to the spatial positions with dominant reflectivities in the observe scene, q=1,2,3,4. We refer readers to [23] for the detailed steps of the standard OMP algorithm. Due to the polarization diversity among the channels, the dominant coefficients at different polarimetric channels may not refer to the same spatial positions in the observed scene. Therefore, to obtain a more consistent interpretation of the observed scene, it is necessary to fuse the sparse solutions at all the polarimetric channels. Here the fusion is carried out by first accumulating pixel-wise all the sparse solutions across all the channels and then selecting K indices corresponding to the largest magnitudes, as expressed in (4). Using the global estimate of the support set, all the local residuals are updated in (5). At each iteration, in (6) the local support set is enlarged by adding K indices selected by OMP based on the local residual, and then in (7) the fusion across all the channels is carried out to select K indices corresponding to the largest projection coefficients. The operations in (6) and (7) are inspired by the backtracking strategy of SP, which aims to find the K-dimensional subspace that the measurement data most likely lie in. In (8), the local residuals are updated by using the global estimate of the support set. When the global recovery error is no longer decreased, iterations over all the polarimetric channels are terminated.

Algorithm 1 The HMP algorithm

Input: $\{\mathbf{s}^{(q)}$, $\mathbf{\Phi}^{(q)}$, for q=1,2,3,4$\}$ and K.

Initialization: Let

$$\Lambda_{old}=\max\_\mathrm{ind}\left(\sum_{q=1}^{Q}\left|\boldsymbol{\sigma}'^{(q)}_{omp}\right|,K\right), \quad (4)$$

where $\boldsymbol{\sigma}'^{(q)}_{omp}=\mathrm{OMP}(\mathbf{s}^{(q)},\mathbf{\Phi}^{(q)},K)$ is the output of the standard OMP algorithm at the q-th polarimetric channel, and the residual vectors

$$\mathbf{r}_{old}^{(q)}=\mathbf{s}^{(q)}-\mathbf{\Phi}_{\Lambda_{old}}^{(q)}\left[\left(\mathbf{\Phi}_{\Lambda_{old}}^{(q)}\right)^H\mathbf{\Phi}_{\Lambda_{old}}^{(q)}\right]^{-1}\left(\mathbf{\Phi}_{\Lambda_{old}}^{(q)}\right)^H\mathbf{s}^{(q)}, \quad (5)$$

for q=1,2,3,4.

Iteration:

1) Let

$$\Lambda_{temp} = \Lambda_{old} \cup \max\_\text{ind}\left(\sum_{q=1}^{Q}\left|\boldsymbol{\sigma}''^{(q)}_{omp}\right|, K\right), \tag{6}$$

where $\boldsymbol{\sigma}''^{(q)}_{omp} = \text{OMP}(\mathbf{r}^{(q)}_{old}, \boldsymbol{\Phi}^{(q)}, K)$.

2) Let

$$\Lambda_{new} = \max\_\text{ind}\left(\sum_{q=1}^{Q}\left|\left[\left(\boldsymbol{\Phi}^{(q)}_{\Lambda_{temp}}\right)^H \boldsymbol{\Phi}^{(q)}_{\Lambda_{temp}}\right]^{-1}\left(\boldsymbol{\Phi}^{(q)}_{\Lambda_{temp}}\right)^H \mathbf{s}^{(q)}\right|, K\right). \tag{7}$$

3) Update the residual vectors as

$$\mathbf{r}^{(q)}_{new} = \mathbf{s}^{(q)} - \boldsymbol{\Phi}^{(q)}_{\Lambda_{new}}\left[\left(\boldsymbol{\Phi}^{(q)}_{\Lambda_{new}}\right)^H \boldsymbol{\Phi}^{(q)}_{\Lambda_{new}}\right]^{-1}\left(\boldsymbol{\Phi}^{(q)}_{\Lambda_{new}}\right)^H \mathbf{s}^{(q)} \tag{8}$$

for q=1,2,3,4.

4) If $\sum_{q=1}^{Q}\left\|\mathbf{r}^{(q)}_{old}\right\|_2^2 > \sum_{q=1}^{Q}\left\|\mathbf{r}^{(q)}_{new}\right\|_2^2$, let $\mathbf{r}^{(q)}_{old} = \mathbf{r}^{(q)}_{new}$ for q=1,2,3,4 and $\Lambda_{old} = \Lambda_{new}$, and return to Step 1; otherwise, stop the iteration and define the sparse solution $\tilde{\boldsymbol{\sigma}} \in \mathbb{C}^{N_x N_y N_z \times 1}$, whose nonzero entries are located at the indices indicated by Λ_{old} with the coefficients

$$\tilde{\boldsymbol{\sigma}}_{\Lambda_{old}} = \sum_{q=1}^{Q}\left|\left[\left(\boldsymbol{\Phi}^{(q)}_{\Lambda_{old}}\right)^H \boldsymbol{\Phi}^{(q)}_{\Lambda_{old}}\right]^{-1}\left(\boldsymbol{\Phi}^{(q)}_{\Lambda_{old}}\right)^H \mathbf{s}^{(q)}\right|. \tag{9}$$

Output: The sparse solution $\tilde{\boldsymbol{\sigma}}$.

In what follows, we discuss the relationship between HMP and existing greedy algorithms. The strategy of local index selection in HMP follows the standard OMP algorithm, i.e., the basis-signals are selected one by one. This helps to guarantee the orthogonality among all the selected basis-signals and, therefore, the capability of distinguishing closely spaced components with a Fourier-like dictionary in (3). The backtracking operations in HMP are similar to that in SP, i.e., at each iteration of HMP, the support set estimate is first enlarged by adding K new candidates and then refined by finding K largest projection coefficients. This makes it possible to remove poor indices chosen at past iterations and add new potential index candidates to the support set estimate. From the above observations, the performance of HMP is expected to be better than that of existing greedy algorithms based on OMP or SP, which is consistent with the experimental results in Section 4.

4. EXPERIMENTAL RESULTS

Radar measurements are collected in the Radar Imaging Lab of the Center for Advanced Communications at Villanova University. A stepped-frequency radar of 1GHz bandwidth centered at 2.5GHz with a frequency step size of 5MHz is used to acquire the full-polarization data. We refer readers to [26] for a detailed description of the experimental setup. In our experiments, the full-polarization data collected at S11 (HH), S12 (HV), S21 (VH), and S22 (VV) channels in the free-space scenario are used to evaluate the proposed HMP algorithm. For each polarization channel, 201 frequency points and 69 azimuth positions are available to acquire data. At the height of 0.73m above the floor, the observed range-azimuth plane is discretized as 121×81 pixels. The results of performing BP on the full data are shown in Fig. 1, where we can see the diversity of the scattering coefficients for different polarimetric channels and the gain of the fusion.

In the following experiment, we randomly select 25 azimuth positions and 30 frequency points from each polarimetric channel and perform different greedy algorithms for fusion of multi-polarization radar images. Thus, the size of $\boldsymbol{\Phi}^{(q)}$ in (2) is 750×9801, for q=1,2,3,4. The sparsity K is set to 70 for all the greedy algorithms. More accurate approaches of choosing the value of K can be found in [21]. Here the methods based on linear programing and Bayesian learning are not considered due to their high computational complexity. The fused images generated by different greedy algorithms are compared in Fig. 2. Each image in Fig. 2 is obtained by randomly selecting subsets of frequency points and azimuth positions and averaging over 50 trials.

From Fig. 2 we can see that HMP outperforms SOMP, SSP and JOMP in the following two aspects: 1) the dominant coefficients in the fused image are more concentrated around the positions of the true targets; and 2) the sizes of the targets are correctly represented in the fused image. The reason why HMP is better than JOMP is that, the accuracy of the majority-vote-based fusion in JOMP may degenerate due to the insufficient number of source images in the scenario of polarimetric radar imaging. To quantitatively evaluate the performances of these algorithms, TCR is used as a measure of quality of the fused images. The definition of TCR is given by

$$TCR = \frac{\sum_{(x,y)\in R_1 \cup R_2 \cdots \cup R_P}\left|I(x,y)\right|^2}{\sum_{(x,y)\notin R_1 \cup R_2 \cdots \cup R_P}\left|I(x,y)\right|^2}, \tag{10}$$

where $\left|I(x,y)\right|^2$ is the magnitude squared of pixel (x, y) of the fused image, P is the number of targets in the observed scene, R_i is the i-th target area consisting of 5×5 pixels around the strongest scatterer of the i-th target. The definition in (10) indicates that a large value of TCR occurs when the targets are accurately located and the clutter and the artifacts outside the target areas are well suppressed.

The values of the TCR of the four algorithms are given in Table 1. As seen in Fig. 2(b), SSP trends to only highlight the two strongest targets and ignores the others. Since the image generated by SSP cannot correctly reflect the true scene, we do not analyze its TCR in Table 1. Compared to SOMP and JOMP, HMP offers better concentration of the dominant coefficients in the fused image and, therefore, a larger value of TCR.

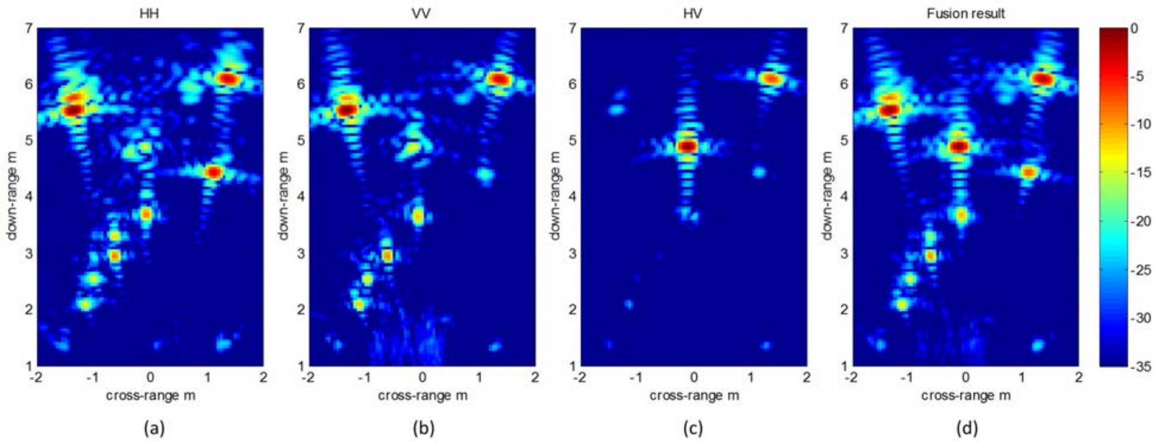

Fig. 1 Multi-polarization images formed by BP: (a) HH, (b) VV, (c) HV/VH, (d) fusion result.

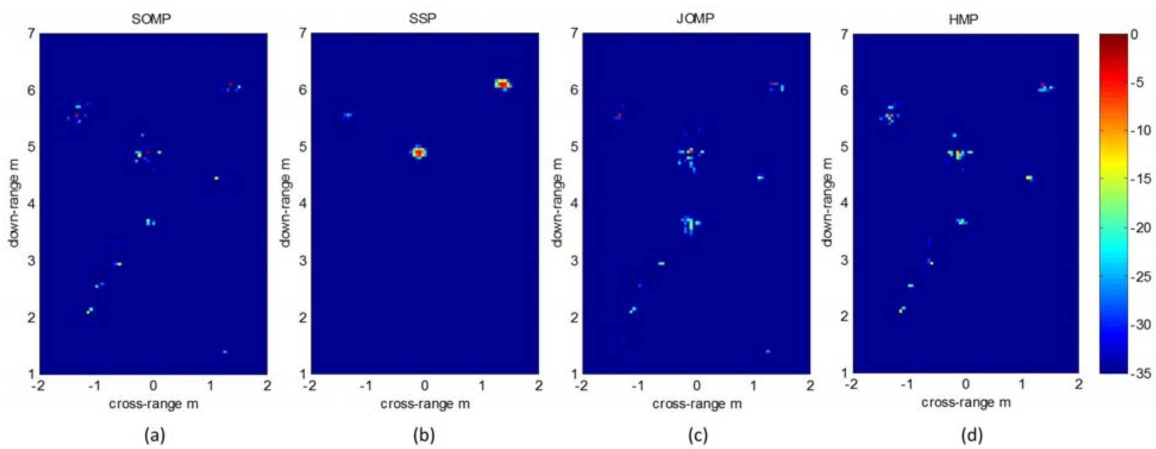

Fig. 2 Fusion results: (a) by SOMP, (b) by SSP, (c) by JOMP, (d) by HMP.

Table 1 TCR of four greedy algorithms

Algorithm	SOMP	SSP	JOMP	HMP
TCR	20.3677	-	28.0066	38.4584

5. CONCLUSION

In this paper, we have developed the HMP algorithm for fusion of multi-polarization radar images by combining the strengths of OMP and SP. Experimental results based on real measured radar data show that HMP can significantly enhance the target reflections and suppress the background clutter. Compared to some popular greedy algorithms, HMP provides better image quality with higher TCR. Future work includes the extension of HMP for target detection and classification with multi-polarization radar.

6. ACKNOWLEDGMENTS

We thank the Center for Advanced Communications at Villanova University for providing the measured radar data used in our experiments.

7. REFERENCES

[1] A. A. Mostafa, C. Debes, and A. M. Zoubir, “Segmentation by Classification for Through-the-Wall Radar Imaging Using Polarization Signatures,” IEEE Transactions on Geoscience and Remote Sensing, vol. 50, no. 9, pp. 3425-3439, Sept. 2012.

[2] C. Debes, A. M. Zoubir, and M. G. Amin, “Enhanced Detection Using Target Polarization Signatures in Through-the-Wall Radar Imaging,” IEEE Transactions on Geoscience and Remote Sensing, vol. 50, no. 5, pp. 1968-1979, May. 2012.

[3] F. Sadjadi, “Improved Target Classification Using Optimum Polarimetric SAR Signatures,” IEEE Transactions on

Aerospace and Electronic Systems, vol. 38, no. 1, pp. 38-49, Jan. 2002.

[4] M. Martorella, E. Giusti, L. Demi, Z. Zhou, A. Cacciamano, F. Berizzi, and B. Bates, "Target Recognition by Means of Polarimetric ISAR Images," IEEE Transactions on Aerospace and Electronic Systems, vol. 47 , no. 1, pp. 225 – 239, Jan. 2011.

[5] P. Yu, A. K. Qin, and D. A. Clausi, "Unsupervised polarimetric SAR image segmentation and classification using region growing with edge penalty," IEEE Transactions on Geoscience and Remote Sensing, vol. 50, no. 4, pp. 1302–1317, Apr. 2012.

[6] R. Paladini, M. Martorella, and F. Berizzi, "Classification of manmade targets via invariant coherency-matrix eigenvector decomposition of polarimetric SAR/ISAR images," IEEE Transactions on Geoscience and Remote Sensing, vol. 49, no. 8, pp. 3022–3034, Aug. 2011.

[7] J.-S. Lee, M. R. Grunes, and E. Pottier, "Quantitative comparison of classification capability: Fully polarimetric versus dual and single polarization SAR," IEEE Transactions on Geoscience and Remote Sensing, vol. 39, no. 11, pp. 2343–2351, Nov. 2001.

[8] D. H. Hoekman and M. A. M. Vissers, "A new polarimetric classification approach evaluated for agricultural crops," IEEE Transactions on Geoscience and Remote Sensing, vol. 41, no. 12, pp. 2881–2889, Dec. 2003.

[9] G. Zhou, Y. Cui, Y. Chen, J. Yang, H. Rashvand, and Y. Yamaguchi, "Linear Feature Detection in Polarimetric SAR Images," IEEE Transactions on Geoscience and Remote Sensing, vol. 49, no. 4, pp. 1453-1463, Apr. 2011.

[10] G. Simonea, A. Farinab, F.C. Morabitoa, S. B. Serpicoc, and L. Bruzzoned, "Image fusion techniques for remote sensing applications," Information Fusion, vol. 3, no. 1, pp. 3-15, Mar. 2002.

[11] C. H. Seng, A. Bouzerdoum, M. G. Amin, S. L. Phung, "Probabilistic Fuzzy Image Fusion Approach for Radar Through Wall Sensing," IEEE Transactions on Image Processing, vol. 22, no. 12, pp. 4938-4951, Dec. 2013.

[12] C. H. Seng, A. Bouzerdoum, M. G. Amin, S. L. Phung, "Two-Stage Fuzzy Fusion With Applications to Through-the-Wall Radar Imaging," IEEE Geoscience and Remote Sensing Letters, vol. 10, no. 4, pp. 687-691, July 2013.

[13] T. Dogaru and C. Le, "SAR Images of Rooms and Buildings Based on FDTD Computer Models," IEEE Transactions on Geoscience and Remote Sensing, vol. 47, no. 5, pp. 1388 – 1401, May 2009.

[14] F. Ahmad and M. Amin, "Multi-location wideband synthetic aperture imaging for urban sensing applications," Journal of the Franklin Institute, vol. 345, no. 6, pp. 618–639, Sep. 2008.

[15] J.R. Orlando, R. Mann, and S. Haykin, "Classification of sea-ice images using a dual-polarised radar," IEEE Journal of Oceanic Engineering, vol. 15, no. 3, pp. 228 – 237. July 1990.

[16] S. Hong, W. Moon, H. Paik, and G. Choi, "Data fusion of multiple polarimetric SAR images using discrete wavelet transform (DWT)," in Proceedings of IEEE International Geoscience and Remote Sensing Symposium (IGARSS), 2002, pp. 3323–3325.

[17] V. H. Tang, A. Bouzerdoum, S. L. Phung, and H. C. Tivive, "Enhanced through-the-wall radar imaging using Bayesian compressive sensing," In Proceedings of SPIE, vol. 8717, May 31, 2013.

[18] Q. Wu, Y. D. Zhang, M. G. Amin, and F. Ahmad, "Through-the-wall radar imaging based on modified Bayesian compressive sensing," IEEE China Summit and International Conference on Signal and Information Processing, Xi'an, China, July 2014.

[19] Q. Wu, Y. D. Zhang, M. G. Amin, and B. Himed, "Multi-static passive SAR imaging based on Bayesian compressive sensing," In Proceedings of SPIE Compressive Sensing Conference, Baltimore, MD, May 2014.

[20] F. H. C. Tivive and A. Bouzerdoum, "A compressed sensing method for complex-valued signals with application to through-the-wall radar imaging," in Proceedings of ICASSP 2014, pp. 2144 – 2148, Vancouver, Canada, May 2014.

[21] J. A. Tropp, A. C. Gilbert, Martin J. Strauss, "Algorithms for simultaneous sparse approximation. Part I: Greedy pursuit," Signal Processing, vol. 86, no. 3, pp. 572-588, Mar. 2006.

[22] W. Dai and O. Milenkovic, "Subspace pursuit for compressive sensing signal reconstruction," IEEE Transactions on Information Theory, vol. 55, no. 5, pp. 2230-2249, May 2009.

[23] J. A. Tropp and A. C. Gilbert, "Signal recovery from random measurements via orthogonal matching pursuit," IEEE Transactions on Information Theory, vol. 53, no. 12, pp. 4655-4666, Dec. 2007.

[24] D. Sundman, S. Chatterjee, and M. Skoglund, "Greedy pursuits for compressed sensing of jointly sparse signals," in Proceedings of the 19th European Signal Processing Conference (EUSIPCO), 2011, pp. 368-372.

[25] J.-M. Feng and C.-H. Lee, "Generalized subspace pursuit for signal recovery from multiple-measurement vectors," in Proceedings of the IEEE Wireless Communications and Networking Conference (WCNC), 2013, pp. 2874-2878.

[26] R. Dilsavor, W. Ailes, P. Rush, F. Ahmad, W. Keichel, G. Titi, and M. Amin, "Experiments on wideband through the wall imaging," in Proc. of the SPIE, Vol 5808, Symposium on Defense and Security, Algorithms for Synthetic Aperture Radar Imagery XII Conference, 2005, pp. 196–209.